Applied Catalysis B: Environmental 181 (2016) 220–227

Contents lists available at ScienceDirect

Applied Catalysis B: Environmental

journal homepage: www.elsevier.com/locate/apcatb

New insight into the enhanced photocatalytic activity of N-, C- and S-doped ZnO photocatalysts

Weilai Yu[a,*], Jinfeng Zhang[b], Tianyou Peng[a,*]

[a] College of Chemistry and Molecular Sciences, Wuhan University, Wuhan 430072, PR China
[b] State Key Laboratory of Advanced Technology for Materials Synthesis and Processing, Wuhan University of Technology, Wuhan 430070, PR China

ARTICLE INFO

Article history:
Received 3 June 2015
Received in revised form 14 July 2015
Accepted 19 July 2015
Available online 26 July 2015

Keywords:
ZnO
Doping
DFT calculation
Band structure
Effective mass

ABSTRACT

In general, N-, C- and S-doped ZnO exhibit much higher phototcatalytic activity than the pure ZnO. However, the essential factors and underlying mechanism regarding the enhancement of photocatalytic activity are still unclear. In this work, the electronic structures, optical properties and effective masses of charge carriers are investigated by first-principle density functional theory calculation. Due to the nature of p-type doping, N and C doping can generate vacant states above the Fermi level and shift the conduction band into lower energy region, resulting in narrowing of band gap. Thus, N- and C-doped ZnO demonstrate much stronger light absorption in both visible and ultraviolet region. In contrast, because of the absence of vacant states, only limited enhancement of light absorption is observed for S-doped ZnO whose improved photocatalytic performance can only be attributed to the direct reduction of band gap. The calculation of the effective masses show that ZnO typically possess light electrons and heavy holes, confirming its intrinsic character of n-type semiconductor, while N, C and S doping can generally render electrons lighter and holes heavier, resulting in slower recombination rate of photogenerated electron–hole pairs. Noticeably, C doping can discourage such recombination to the greatest extent and separate electron–hole pairs most efficiently compared with N and S doping, serving as a potentially promising pathway to increase the quantum efficiency of ZnO-based photocatalysts. This work will provide some new insights into the understanding of doping effect over the enhancement of photocatalytic activity of N-, C- and S-doped ZnO.

1. Introduction

As is well known, semiconductor-based heterogeneous photocatalysis is regarded as a promising solution to deal with the increasingly serious environmental [1–3] and energy-related issues [4–8] worldwide. Since Fujishima and Honda first achieved photoinduced water splitting by coupling TiO_2 and Pt photoelectrodes in a photoelectrochemical cell in 1972 [9], a great deal of efforts have been concentrated on developing highly active semiconductor-based photocatalysts, including various metal oxides (TiO_2 [10–13], ZnO [14], WO_3 [15,16], etc.) and metal sulfides (ZnS [17,18] and CdS [19–21], etc.). Among them, ZnO has been intensively studied in the past decade, due to its fascinating features such as high photosensitivity [22], biocompatibility [23] and low cost [24]. With a direct band gap and band edge positions both similar as that of TiO_2, ZnO demonstrates 10–100 folds higher electron mobility than TiO_2, and thus reduced electrical resistance and enhanced electron transfer efficiency [25]. Therefore, ZnO has been proven to be a competitive candidate for a wide range of photocatalytic and photoelectrochemical applications [26–29]. However, the wide intrinsic band gap of ZnO (3.2 eV) allows the absorption of only ultraviolet (UV) light, which corresponds to 4% of solar spectrum. This largely impairs the utilization of visible light which makes up as much as 43% of solar spectrum [30]. In this regard, reducing the band gap of ZnO toward better utilization of solar spectrum has become one of the most significant goals in the development of efficient ZnO-based photocatalysts.

Till now, a great number of methods have been employed to narrow the band gap of ZnO and shift its light absorption spectrum into lower energy region [31–36]. Among these methods, band gap engineering through metal or nonmetal doping is considered as one of the most effective strategies and has been widely adopted [37–40]. Particularly, due to the generally smaller atomic size of nonmetal elements, nonmetal doping into ZnO lattice is usually much easier to be carried out experimentally than metal doping. In contrast,

* Corresponding authors.
E-mail addresses: yuweilai93@aliyun.com (W. Yu), typeng@whu.edu.cn (T. Peng).

http://dx.doi.org/10.1016/j.apcatb.2015.07.031
0926-3373/

metal doping is more likely to induce the formation of vacancies or defect states that can serve as the recombination center for photogenerated electrons and holes. Compared with other nonmetal dopants, nitrogen [41–46], carbon [47–51] and sulfur [52–54] have been more extensively studied in recent years. Doping ZnO with these nonmetal elements has shown to be promising approaches to narrow the band gap and thus induce stronger visible-light absorption. For instance, Liu et al. have fabricated a hierarchical flower-like C-doped ZnO superstructure exhibiting enhanced photocatalytic activity, which can be attributed to the effect of doping carbon atoms into the ZnO lattice [50]. More recently, Xu et al. have synthesized visible-light responsive N-doped ZnO nanobundles showing much higher activity for water oxidation reaction upon visible-light irradiation [30].

Although a variety of N-, C- and S-doped ZnO nanostructures with enhanced photocatalytic activities have been investigated experimentally, up till now, there are only few related theoretical studies to probe the detailed mechanism and essential factors underlying these doping effects. Obviously, the origin of the enhancement of photocatalytic activity of these non-metal doped ZnO still remains unclear. To the best of our knowledge, doping these atoms in appropriate positions of the ZnO lattice is able to considerably alter both geometric and electronic structures, which can primarily determine their optical properties and corresponding photocatalytic activity. Moreover, the effective masses of the photogenerated charge carriers can also exert significant influence over the mobility, transfer and separation of photogenerated electrons and holes [55]. Therefore, in this regard, a systematic investigation on the doping effect in terms of electronic structures, optical properties and effective masses of charge carriers of these non-metal doped ZnO photocatalysts is urgently necessary for a better understanding of their promotion of photocatalytic activity. Moreover, until lately, there is almost no relevant research that has emphasized on the influence of charge carrier effective mass over the enhanced photocatalytic activity of N-, C- and S-doped ZnO.

Herein, for the first time, we systematically investigate the electronic structures, optical properties and effective masses of charge carriers of N-, C- and S-doped ZnO photocatalysts. The crystal structures, total and projected density of states (DOS), band structures and optical properties of N-, C- and S-doped ZnO were first calculated by employing first-principle density functional theory (DFT). More importantly, based on the results of theoretical calculation, the effective masses of photogenerated electrons and holes of both pure and doped ZnO are also calculated. Furthermore, the calculated electronic structures, optical properties and effective masses are all applied to discuss and explain their corresponding enhanced photocatalytic activity. This work will provide new insight into the underlying essential factors and detailed mechanism regarding the enhancement of photocatalytic activity for N-, C- and S-doped ZnO and inspire the design and synthesis of highly efficient ZnO-based photocatalysts.

2. Computational details

All DFT calculations in the present work were performed on CASTEP code based on the plane-wave pseudopotential method [56]. The generalized gradient approximation (GGA) with the Perdew–Burke–Ernzerhof (PBE) was used as the exchange-correlation function [57,58]. The ultrasoft pseudopotential was used to describe the interaction between the ionic core and valence electrons. The lattice parameters and atomic coordinates were relaxed using the cutoff energy of 380 eV and Monkhorst-pack grids of $4 \times 4 \times 2$ k-points for both pure and doped ZnO models. Geometric optimization was first achieved using convergence thresholds of 2×10^{-5} eV per atom for total energy, 0.03 eV Å^{-1} for maximum force, 0.05 GPa for pressure, and 0.001 Å for maximum displacement. The self-consistent calculations were performed with a total tolerance of less than 1×10^{-6} eV per atom. The valence electrons taken into account for ZnO correspond to: $Zn3p^6 3d^{1\circ} 4s^2$ and O $2s^2 2p^4$, while the remaining electrons are kept frozen as core states. In order to confirm the accuracy of these calculations, we adopted higher cutoff energy and more k-points, the results of which showed almost no change in terms of total energy and geometric parameters. After the geometric optimizations were finished, the band structures, total and projected DOS, optical properties were obtained and the effective masses of charge carriers were calculated based on the obtained electronic structures.

Since the hexagonal wurtzite ZnO is considered as the most stable and common phase of ZnO under ambient conditions, a $2 \times 2 \times 2$ hexagonal wurtzite ZnO supercell was constructed. In order to simulate the effect of different doping patterns inside the ZnO supercell, geometric optimizations were performed to cover all the three doping patterns: (1) O-substituted, (2) Zn-substituted and (3) interstitially occupied doping models under the same calculation conditions, respectively. As expected, the final results indicate that O-substituted doping usually generates ignorable change to lattice parameters, while either the Zn-substituted or interstitially occupied doping pattern might result in large lattice distortion and unreasonably high formation energy. As a consequence, self-consistent relaxation of the latter two doping patterns typically took extremely long time to accomplish compared with the O-substituted models. Based on these facts, we can rationally assume that it is generally much easier for the doping of nitrogen, carbon and sulfur atoms to take place at the position of oxygen atom inside ZnO lattice, due to their reasonable lattice alteration and formation energy. This can be mainly attributed to the similarity of atomic radius and eletronegativity between these non-metal atoms and O atoms as compared to Zn atoms. In this regard, for both simplicity and clarity, only the O-substituted doping patterns in the hexagonal wurtzite ZnO structures were considered and further discussed in the present work.

3. Results and discussions

3.1. Crystal structures and formation energy

The optimized crystal structures of $2 \times 2 \times 2$ supercells of pure (a), N- (b), C- (c) and S- (d) doped ZnO are shown in Fig. 1. Comparison between the crystal structures of pure and doped ZnO reveals that the substitution of one oxygen atom with another nitrogen, carbon or sulfur atom in each supercell generates almost no significant change inside the crystal lattice. The geometric parameters of different supercells are shown in Table 1 and their corresponding formation energies are also calculated based on the total energy of the optimized crystal structures and chemical potentials of different doping atoms. The following Eq. (1) is employed in the calculation of formation energy [59,60]:

$$E_{\text{form}} = E_{\text{doped}} - E_{\text{pure}} - m\mu_{\text{N}} - n\mu_{\text{C}} - k\mu_{\text{s}} + x\mu_{\text{O}} \quad (1)$$

Where E_{doped} and E_{pure} are the total energy of the doped and pure ZnO supercell, respectively. μ_{N} (μ_{C}, μ_{s} and μ_{O}) is the chemical potentials of N (C, S and O) atoms. The coefficients m, n and k are the number of N, C and S atoms doped into the supercells of ZnO, respectively. The x represents the numbers of O atoms substituted by impurity atoms. The relationships between chemical potentials of oxygen and other impurity atoms (nitrogen, carbon and sulfur) are as follows:

$$\mu_{\text{O}} = 1/2\mu(\text{O}_2),\ \mu_{\text{N}} = 1/2\mu(\text{N}_2) \quad (2)$$

$$2\mu_{\text{O}} + \mu_{\text{C}} = \mu(\text{CO}_2) \quad (3)$$

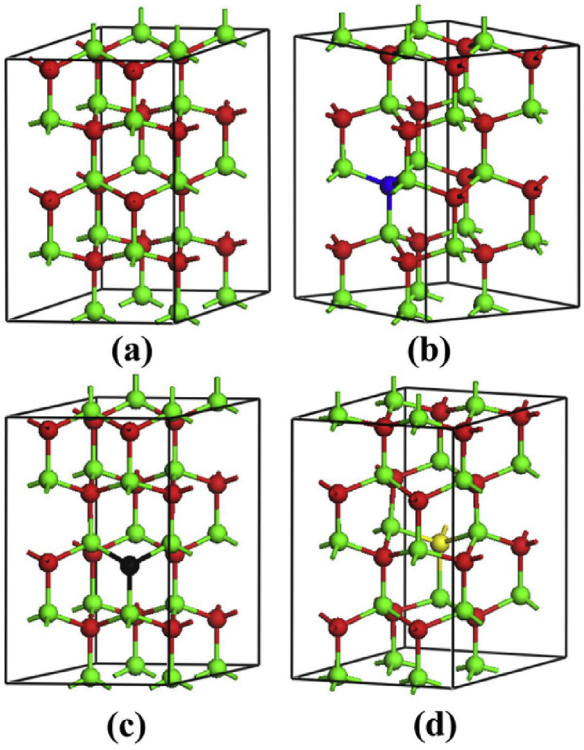

Fig. 1. Schematic illustration of the optimized crystal structures of $2 \times 2 \times 2$ supercells for pure (a), N-doped (b), C-doped (c), S-doped (d) ZnO; The green and red balls represent zinc and oxygen atoms, respectively; The blue (b), black (c), yellow (d) balls stand for the doped nitrogen, carbon and sulfur atoms, respectively. (For interpretation of the references to color in this figure legend, the reader is referred to the web version of the article.)

$$2\mu_O + \mu_S = \mu(SO_2) \quad (4)$$

As can be seen from Table 1, the optimized crystal structures of all three doped ZnO models have nearly the same structure parameters compared with pure ZnO, confirming the relative stability of nitrogen, carbon and sulfur dopants inside the ZnO lattice and the corresponding feasibility of doping in substitution of O atoms compared with replacing Zn atoms or occupying interstitially. However, all N-, C- and S-doped models demonstrate a slight tendency to elongate along the c crystal direction. In particular, S doping causes relatively larger lattice expansion, mainly due to the larger atomic radius of sulfur atoms compared with that of oxygen atoms.

The calculated results of formation energy indicate that the substitution of oxygen atoms with the other three doping atoms needs external energy input, which is required to generate the slight deviation of structure parameters from the pure ZnO. Among the three doping models, the C doping needs the largest energy input (12.0 eV), which is due to the most significant electronically deficient character of carbon atoms. In contrast, N doping demands the least energy input (4.7 eV) because of the greatest similarity between nitrogen and oxygen atoms in terms of both atomic radius and electronegativity. The doping of sulfur atoms also requires a considerable amount of energy input (7.0 eV), most of which originates from the much larger atomic radius of sulfur atoms.

3.2. Electronic structures

To analyze the modifications of doping effect on electronic structures and clarify the origin of the enhancement of photocatalytic activities of these non-metal doped ZnO, both the DOS and band structures were calculated based on the optimized crystal structures shown in Fig. 1.

Firstly, both the total and corresponding projected DOS of pure and doped ZnO are demonstrated simultaneously in Fig. 2. Considering the DOS of pure ZnO, the valence band mainly consists of O 2p states and Zn 3d states, with only a limited contribution from Zn 3p states. Thus, the hybridization of O 2p states and Zn 3d states, which respectively occupy the upper and lower part of the valence band, form the bonding states in this energy region. The conduction band of ZnO is mainly composed of Zn 3p and 4s states with nearly equal contribution, mixed with a few O 2s states. In this regard, the anti-bonding states in the conduction band of ZnO is almost totally constituted by the electronic states from Zn atoms and unlike TiO_2, hybridization between the two different elements is not observed in conduction band region of ZnO [62].

The results show that the total DOS of both pure and doped ZnO generally have apparently similar distributions of elemental electronic states. Compared with the DOS of pure ZnO, the contributions of electronic states from nitrogen, carbon and sulfur atoms to the valence band of ZnO all come from their corresponding 2p, 2p and 3p states, respectively. In contrast, since the conduction band is mainly composed of electronic states from Zn atoms, these doping atoms show ignorable influence over the composition of the conduction band. However, a deeper investigation informs us that doping nitrogen, carbon and sulfur atoms in substitution of oxygen atoms can indeed alter the near-Fermi level DOS of ZnO and their corresponding electronic structures in different ways. It is widely recognized that electronic structures near the Fermi level of a semiconductor can have a major influence over its physical properties and photocatalytic activity. In order to facilitate the comparison of different doping effects near the Fermi level, detailed distributions of DOS in the near-Fermi level region are provided in Fig. 3.

As shown in Fig. 3, the Fermi level of pure ZnO is mostly populated by O 2p states. Due to the similarity of atomic size and electronegativity with oxygen atoms, the N 2p states and C 2p states are both located closer to the Fermi level of the doped ZnO than the S 3p states, most of which are far below the Fermi level. The differences of electronic energy level between the doping atoms and original oxygen atoms can significantly alter the near-Fermi level electronic properties. Compared with the total electron density at the Fermi level of pure ZnO (5.10 electrons/eV), the emergence of N 2p and C 2p states near the Fermi level can both increase the electron density to 7.29 electrons/eV and 7.04 electrons/eV, respectively. Since the Fermi level represents the very top of the valence band containing the electrons with the highest energy at ground state, the increase of the total electron density at the Fermi level can be beneficial to elevate the population density of photogenerated electrons and holes upon excitation.

Table 1
Comparison of geometric parameters and formation energy based on the optimized crystal structures of pure and N-, C-, S-doped ZnO.

Species	a (Å)	b (Å)	c (Å)	Formation energy (eV)
Pure ZnO	3.281 (3.249[a])	3.281 (3.249[a])	5.315 (5.207[a])	–
N-doped ZnO	3.272	3.272	5.337	4.7
C-doped ZnO	3.263	3.263	5.383	12.9
S-doped ZnO	3.312	3.312	5.388	7.0

[a] See Ref. [61]

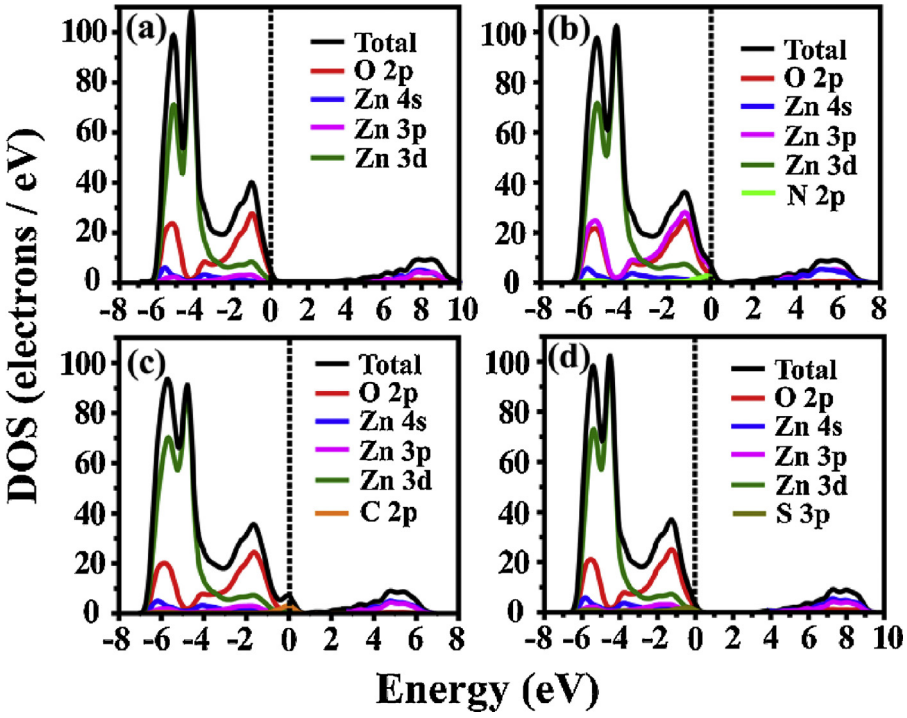

Fig. 2. Comparison of total and projected density of states of pure (a), N-doped (b), C-doped (c), S-doped (d) ZnO.

It should be noted that the C 2p states have a relatively greater contribution (3.16 out of 7.04 electrons/eV) to the increase of the total electron density at the Fermi level compared with that of N 2p states (2.35 out of 7.29 electrons/eV), which is also even more significant than the original O 2p states. However, interestingly, the doped nitrogen atoms can not only considerably increase the Fermi level electron density by itself, but also can elevate the contributions of the Zn 3p states in the entire valence band on a large scale. As indicated in both Figs. 2 and 3, N doping can increase the contribution of Zn 3p states in the whole valence band region to an extent comparable to O 2p states, while most of the Zn 3p states in pure ZnO are still located in the conduction band. This possibly

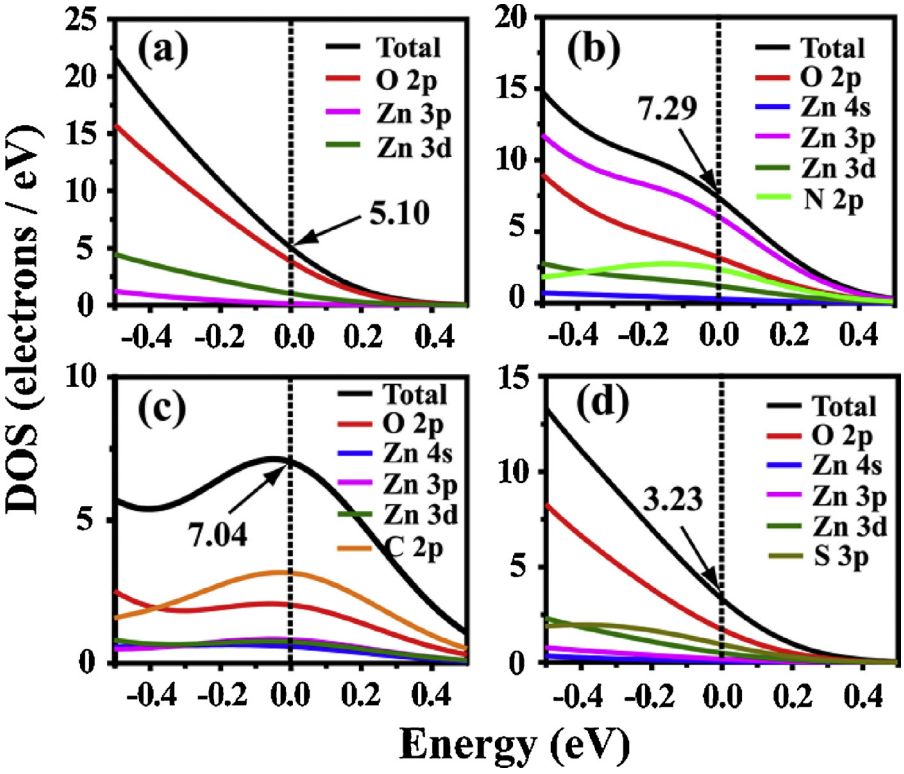

Fig. 3. Comparison of detailed distribution of density of states (DOS) near the Fermi level of pure (a), N-doped (b), C-doped (c), and S-doped (d) ZnO.

suggests a better overlap between N 2p orbitals and Zn 3p orbitals due to a higher degree of compatibility of electronic energy levels and orbital sizes. This better overlap of N doping might lead to a wider dispersion of both valence and conduction bands with greater width so as to decrease the band gap in between. Notably, Fig. 2b and c shows that the conduction bands of N- and C-doped ZnO both shift toward lower energy region compared with that of pure ZnO, indicating band gap narrowing and wider coverage of light absorption range. Moreover, this elevation of the Zn 3p states also has a remarkable contribution to the increase of the Fermi level electron density in N-doped ZnO.

In terms of electronic structures, nitrogen ($2s^2 2p^3$) and carbon ($2s^2 2p^2$) are both considered as electronically deficient in comparison with oxygen ($2s^2 2p^4$), while sulfur ($3s^2 3p^4$) and oxygen ($2s^2 2p^4$) are much more alike because of their same number of valence electrons. In this regard, doping nitrogen or carbon atoms at the place of oxygen is expected to be p-type doping that is usually well characterized by the formation of vacant states slightly above the Fermi level [41,63,64]. The emergence of vacant states can be simultaneously attributed to both the deficiency of electrons and lower electronegativity (higher energy level of valence orbitals) of nitrogen or carbon than those of oxygen. Actually, the distribution of near-Fermi level DOS in Fig. 3 confirms this point of view. As shown in Fig. 3, the appearance of N 2p and C 2p states can not only increase the Fermi level electron density, but also create more vacant states extending into the region slightly over the Fermi level. In this way, it is much easier for electrons at Fermi level to jump into higher energy region through thermal excitation by making use of these available vacant states [65]. Thus, the additional expansion of valence band from the generation of vacant states can serve as an efficient pathway to narrow the band gap and induce wider range of light absorption. Because sulfur contains the same number of valence electrons as oxygen, neither of the increase of Fermi level electron density (3.23 electrons/eV) nor the extension of the valence band is observed in the total and projected DOS of the S-doped ZnO, which is confirmed by the similarity of their DOS distributions. From this perspective, S doping can only generate limited modifications to both total and projected density of states of ZnO compared with N or C doping.

The energy band structures of both pure and doped ZnO along the high symmetry directions in the Brillouin zone were also calculated, as shown in Fig. 4. The Fermi level, shown by a dashed line in Fig. 4, is set as zero in energy level. It can be seen that all pure and doped ZnO belong to the category of direct band-gap semiconductor, confirming the results of experimental measurements. Both of the valence band maximum (VBM) and the conduction band minimum (CBM) are located at G point. The calculated band gap of pure ZnO is 0.73 eV, which is much lower than the experimental value of 3.2 eV. This is mainly owing to the well-known shortcoming of the GGA function in DFT calculation [66].

It should be noted that, in comparison with the band structure of pure ZnO, impurity states emerge in the band gap of both N- and C-doped ZnO, while no such impurity states appear in the band gap of S-doped ZnO. This is consistent with the previous discussions of DOS distribution. Due to the p-type doping character of N or C doping, vacant states are introduced into the band gap over the Fermi level, extending the valence band into higher energy region. By taking advantage of thermal excitation, such extension over the Fermi level can function as a "springboard" for electrons to jump into the conduction band, which can reduce band gap, and induce stronger and wider light absorption and eventually enhance photocatalytic activity.

As denoted clearly in Fig. 4, the gaps between the impurity states and CBM in N- and C-doped ZnO are 0.58 eV and 0.16 eV, respectively. Both of these values are considerably less than the calculated value of band gap for pure ZnO (0.73 eV). Thus, these gap states can

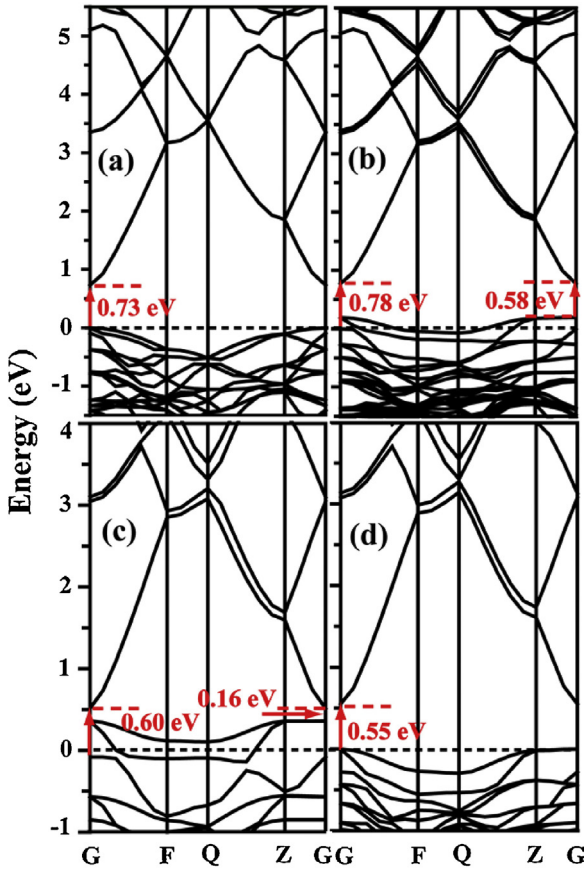

Fig. 4. Comparison of band structures and possible excitation energy of pure (a), N-doped (b), C-doped (c) and S-doped (d) ZnO.

serve as the abovementioned "springboard" to reduce the demands of photon energy and efficiently facilitate the excitation of photogenerated electrons. The lower value of the gap between the impurity states and CBM in the C-doped ZnO indicates the relatively higher energy of carbon impurity states than nitrogen impurity states of N-doped ZnO. This is mainly due to the lower electronegativity and more electron-deficient character of carbon atoms in contrast to those of nitrogen atoms. Furthermore, the gap between the Fermi level and CBM in C-doped ZnO also decreases to 0.60 eV, while it slightly increases to 0.78 eV in N-doped ZnO. Thus, we can reasonably propose that C doping might have a stronger influence on the band structures than N doping by simultaneously narrowing the Fermi level-CBM gap and introducing gap states with higher energy into the band gap of ZnO.

Noticeably, although there are no impurity states observed in the band structures of S-doped ZnO, its band gap still decreases to 0.55 eV, which is also lower than that of pure ZnO. This direct reduction of band gap value might indicate that the enhanced photocatalytic activity of S-doped ZnO, which was experimentally proved, may actually originate from the direct narrowing of the band gap between VBM and CBM. Further comparison of both DOS and band structures reveals that it is the comparatively moderate shift of the entire conduction band toward lower energy region that might account for the narrowing of the band gap and further enhancement of photocatalytic activity of S-doped ZnO.

3.3. Optical properties

In order to simulate the absorption spectra of both pure and doped ZnO, optical properties of both pure and doped ZnO were also calculated based on polycrystalline model. A scissor energy of

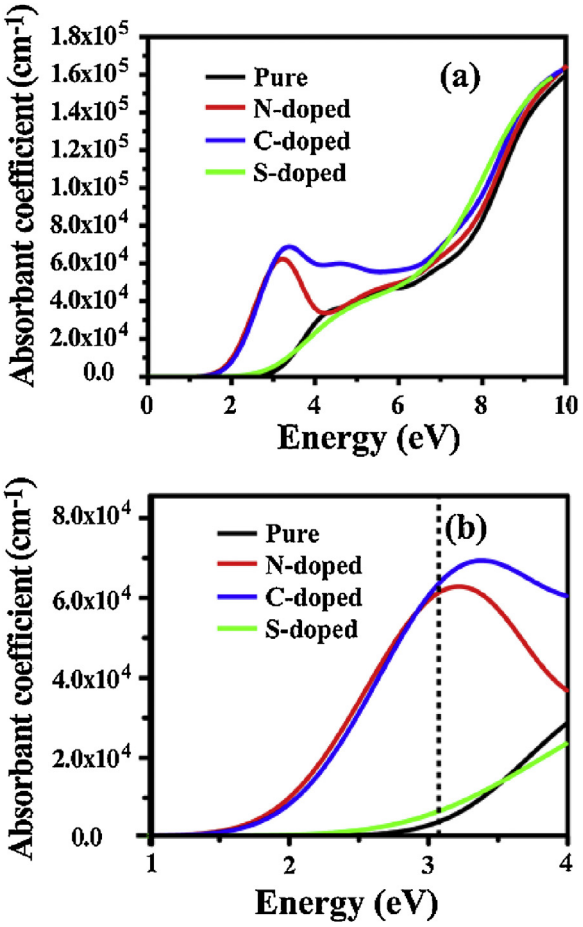

Fig. 5. Comparison of simulated light absorption spectra of pure (black), N-doped (red), C-doped (blue), S-doped (green) ZnO in all spectra (a), and visible and near ultraviolet light region (b). The vertical dashed line at 3.1 eV designates the boundary between visible and ultraviolet light. (For interpretation of the references to color in this figure legend, the reader is referred to the web version of the article.)

2.47 eV is applied in the calculation in order to compensate for the gap between the theoretical value (0.73 eV) and experimental value (3.20 eV) of the pure ZnO band gap. The final results are shown in the Fig. 5. A vertical dashed line at the energy level of 3.1 eV (wavelength = 400 nm) is indicated to distinguish the boundary between visible light and ultraviolet light.

Fig. 5a shows that the absorption edge of both N- and C-doped ZnO shift into much lower energy region as compared to S-doped and pure ZnO. The absorption coefficients for both N- and C-doped ZnO are both elevated to great extent in both visible and ultraviolet light region, indicating effective narrowing of band gap and much stronger light absorption features. As shown in Fig. 5b, the absorption bands of N- and C-doped ZnO are similar in visible light region, while C-doped ZnO demonstrates even stronger absorption in the near-ultraviolet region than N-doped ZnO. In this regard, C-doped ZnO can be considered to possess the most intense light absorption in the whole spectrum. More careful comparison in Fig. 5b also reveals that the absorption band of the S-doped ZnO lies slightly above that of the pure ZnO in both visible light and ultraviolet light region, indicating that S doping has limited effect on the enhancement of light absorption.

The above results of simulated optical properties match well with the previous discussions of electronic structures in Section 3.2. The N and C doping can modify the optical properties of ZnO to more considerable degree, mainly due to the effect of p-type doping characters on their electronic structures. The S doping can only produce moderate enhancement of light absorption because only the direct band gap narrowing is observed in the electronic structures of the S-doped ZnO. Combining optical and electronic properties together, it can be confirmed that N and C doping in ZnO lattice could be much more effective to induce stronger light absorption in both visible and near-ultraviolet light region. Such doping patterns are beneficial for overcoming the wide intrinsic band gap of pure ZnO and further enhancing the photocatalytic activity of ZnO under normal solar irradiation.

3.4. Effective mass of photogenerated electrons and holes

As widely recognized, after the generation of coloumbically bound electron–hole pairs upon light excitation, the relative transfer rate of photogenerated electrons to holes plays a dominant role in the determination of quantum efficiency for various photocatalytic reactions. The transfer rate of the photogenerated electrons and holes can be directly evaluated by their effective masses, which can be explained in the following formula [59,60]:

$$v = \hbar k / m* \quad (5)$$

where m^* is the effective mass of charge carrier, k is the wave vector, $\hbar$ is the reduced Planck constant and v is the transfer rate of photogenerated electrons and holes. In general, the transfer rate is inversely proportional to the effective masses of electrons and holes. In other words, lighter charge carriers will move faster.

As is well known, the photocatalytic activity of various photocatalysts suffers greatly from the bulk recombination of the photogenerated electrons and holes. In fact, the recombination rate of the photogenerated electrons and holes are directly determined by their relative transfer rates. The greater discrepancy of transfer rates between photogenerated electrons and holes typically corresponds to their faster separation and slower recombination rates. Since the transfer rates of charge carriers are directly related to their effective masses, it is reasonable to apply effective mass to evaluate the recombination rate of electrons and holes. In order to investigate the differences of photocatalytic activity among pure and doped ZnO, the effective mass of electrons (m_e^*) and holes (m_h^*) along the designated directions were calculated respectively, by fitting parabolic functions around the CBM or the VBM according to the following equation:

$$m^* = \hbar^2 (d^2E/dk^2)^{-1} \quad (6)$$

where m^* is the effective mass of charge carrier, k is the wave vector, $\hbar$ is the reduced Planck constant, and E is the energy of an electron at wavevector k in that band. To acquire the validity of the parabolic approximation within the VBM and CBM regions, the region for parabolic fitting is controlled within an energy difference of 1 meV along a particular direction around the VBM or CBM. The same method is also used in other research works to calculate the effective mass of charge carriers. The obtained results of effective masses of both photogenerated electrons and holes are summarized in Table 2 [67].

The calculated results demonstrate that in both pure and doped ZnO, photogenerated electrons are much lighter than their corresponding holes, indicating that ZnO belongs to the type of semiconductor with light photogenerated electrons and heavy photogenerated holes. This agrees well with the fact that ZnO is intrinsically n-type semiconductor. Interestingly, compared with pure ZnO, the photogenerated electrons and holes in N-, C- and S-doped ZnO all become lighter and heavier, respectively. Such combination of lighter electrons and heavier holes in doped ZnO is undoubtedly beneficial for the separation of photogenerated electrons and holes, and further enhances their photocatalytic activity. Based on the above discussion, this is because larger differences

Table 2
The effective masses of electrons and holes for both pure and doped ZnO obtained from parabolic fitting to CBM and VBM along a specific direction in the reciprocal space.

Species	Effective mass	G → Z	G → F
Pure ZnO	m_h^*/m_0	0.717	0.899
	m_e^*/m_0	0.034	0.077
	D	**21.1**	**11.7**
N-doped ZnO	m_h^*/m_0	2.194	2.714
	m_e^*/m_0	0.033	0.077
	D	**66.5**	**35.2**
C-doped ZnO	m_h^*/m_0	13.755	4.188
	m_e^*/m_0	0.029	0.058
	D	**474.3**	**72.2**
S-doped ZnO	m_h^*/m_0	1.829	1.497
	m_e^*/m_0	0.033	0.074
	D	**55.4**	**20.2**

Bold values are used to emphasize the definition of relative effective mass referring to the differences of effective masses of photogenerated electrons and holes of pure and doped ZnO.

of the effective mass between electrons and holes will result in larger differences of transfer mobility and slower recombination rates of the photogenerated electron–hole pairs. For clarity, a definition regarding the relative effective mass of electron–hole pairs is employed according to the following equation, to evaluate the corresponding recombination rate and photocatalytic activity for both pure and doped ZnO [68]

$$D = m_h^*/m_e^* \quad (7)$$

where D is defined as the relative effective mass, m_h^* and m_e^* are the effective mass of photogenerated electrons and holes, respectively. Based on the above-mentioned discussions, a higher value of D usually indicates slower recombination rate and higher photocatalytic activity. The calculated values of D are also summarized in Table 2.

The results show that the values of D in the direction from G to Z are generally higher than the direction from G to F in both pure and doped ZnO. Moreover, the values of D in all doped ZnO are higher than that of pure ZnO in both directions, suggesting that the doping effect can lead to slower recombination rate of electrons and holes. In particular, it can be observed that C doping can increase the D value to much greater extent than either N or S doping, and the effect of N doping on the D value is a little higher than S doping. Therefore, according to the calculation results, the recombination rates of electron–hole pairs in both pure and doped ZnO follow the order as: C-doped « N-doped < S-doped < pure ZnO. From this perspective, C doping can be considered as one of the most efficient routes to retard the bulk recombination of photogenerated electron–hole pairs in ZnO.

4. Conclusions

The electronic structures, optical properties and effective masses of charge carriers of pure, N-, C- and S-doped ZnO are calculated based on plane-wave pseudopotential method of DFT calculation. The electronic structures show that the valence band of pure ZnO is mostly composed of Zn 3d states (lower) and O 2p states (upper), while the conduction band is equally populated by Zn 4s and 3p states. Both N and C doping have two major effects: (1) increasing the Fermi level electron density and (2) introducing vacant (impurity) states into the band gap, mainly due to their nature of p-type doping. The introduced impurity states by N and C doping can facilitate the excitation of electrons and moreover, C doping can also reduce the gap between the Fermi level and conduction band. Without the emergence of vacant states, the enhanced photocatalytic activity of S-doped ZnO is attributed to direct band gap narrowing. The calculation of optical properties reveals that much stronger light absorption of visible and ultraviolet light can be induced by N and C doping. Notably, C-doped ZnO demonstrates the most intense light absorption over the whole spectrum, originating from its most significant electronically deficient character. The calculated effective masses of charge carriers show that as an n-type semiconductor, ZnO contains light electrons and heavy holes. Upon N, C or S doping, the photogenerated electrons and holes all become lighter and heavier, respectively. The recombination rates of photogenerated electron–hole pairs are evaluated as C doping « N doping < S doping < pure ZnO. These theoretical investigations may provide new insights into the fundamental understanding of the underlying mechanism for the enhanced photocatalytic activity of N-, C- and S-doped ZnO.

Acknowledgement

This work was supported by the Natural Science Foundation of China (21271146, 20973128).

References

[1] C. Chen, W. Ma, J. Zhao, Chem. Soc. Rev. 39 (2010) 4206–4219.
[2] M. Pelaez, N.T. Nolan, S.C. Pillai, M.K. Seery, P. Falaras, A.G. Kontos, P.S.M. Dunlop, J.W.J. Hamilton, J.A. Byrne, K. O'Shea, M.H. Entezari, D.D. Dionysiou, Appl. Catal. B: Environ. 125 (2012) 331–349.
[3] N. Serpone, A.V. Emeline, J. Phys. Chem. Lett. 3 (2012) 673–677.
[4] X. Chen, S. Shen, L. Guo, S.S. Mao, Chem. Rev. 110 (2010) 6503–6570.
[5] X. Li, J. Wen, J. Low, Y. Fang, J. Yu, Sci. China Mater. 57 (2014) 70–100.
[6] X. Li, J. Yu, J. Low, Y. Fang, J. Xiao, X. Chen, J. Mater. Chem. A 3 (2015) 2485–2534.
[7] M. Marszewski, S. Cao, J. Yu, M. Jaroniec, Mater. Horiz. 2 (2015) 261–278.
[8] J. Ran, J. Zhang, J. Yu, M. Jaroniec, S.Z. Qiao, Chem. Soc. Rev. 43 (2014) 7787–7812.
[9] A. Fujishima, K. Honda, Nature 238 (1972) 37–38.
[10] X. Chen, L. Liu, P.Y. Yu, S.S. Mao, Science 331 (2010) 746–750.
[11] G. Liu, L.-C. Yin, J. Wang, P. Niu, C. Zhen, Y. Xie, H.-M. Cheng, Energy Environ. Sci. 5 (2012) 9603–9610.
[12] Q. Xu, J. Yu, J. Zhang, J. Zhang, G. Liu, Chem. Commun. 51 (2015) 7950–7953.
[13] J. Yu, J. Low, W. Xiao, P. Zhou, M. Jaroniec, J. Am. Chem. Soc. 136 (2014) 8839–8842.
[14] Y. Wang, R. Shi, J. Lin, Y. Zhu, Energy Environ. Sci. 4 (2011) 2922–2929.
[15] J. Kim, C.W. Lee, W. Choi, Environ. Sci. Technol. 44 (2010) 6849–6854.
[16] Q. Mi, Y. Ping, Y. Li, B. Cao, B.S. Brunschwig, P.G. Khalifah, G.A. Galli, H.B. Gray, N.S. Lewis, J. Am. Chem. Soc. 134 (2012) 18318–18324.
[17] Y. Zhang, N. Zhang, Z.-R. Tang, Y.-J. Xu, ACS Nano 6 (2012) 9777–9789.
[18] D. Chen, F. Huang, G. Ren, D. Li, M. Zheng, Y. Wang, Z. Lin, Nanoscale 2 (2010) 2062–2064.
[19] Q. Li, B. Guo, J. Yu, J. Ran, B. Zhang, H. Yan, J.R. Gong, J. Am. Chem. Soc. 133 (2011) 10878–10884.
[20] Q. Li, X. Li, S. Wageh, A.A. Al-Ghamdi, J. Yu, Adv. Energy Mater. (2015), http://dx.doi.org/10.1002/aenm.201500010
[21] J. Yu, Y. Yu, P. Zhou, W. Xiao, B. Cheng, Appl. Catal. B: Environ. 156–157 (2014) 184–191.
[22] H. Chang, Z. Sun, K.Y. Ho, X. Tao, F. Yan, W.M. Kwok, Z. Zheng, Nanoscale 3 (2011) 258–264.
[23] C. Dagdeviren, S.W. Hwang, Y. Su, S. Kim, H. Cheng, O. Gur, R. Haney, F.G. Omenetto, Y. Huang, J.A. Rogers, Small 9 (2013) 3398–3404.
[24] A. Manekkathodi, M.Y. Lu, C.W. Wang, L.J. Chen, Adv. Mater. 22 (2010) 4059–4063.
[25] H.M. Chen, C.K. Chen, Y.C. Chang, C.W. Tsai, R.S. Liu, S.F. Hu, W.S. Chang, K.H. Chen, Angew. Chem. 49 (2010) 5966–5969.
[26] H.-M. Cheng, W.-F. Hsieh, Energy Environ. Sci. 3 (2010) 442–447.
[27] Y. Qiu, K. Yan, H. Deng, S. Yang, Nano Lett. 12 (2012) 407–413.
[28] J. Tian, Q. Zhang, E. Uchaker, R. Gao, X. Qu, S. Zhang, G. Cao, Energy Environ. Sci. 6 (2013) 3542–3547.
[29] W.W. Zhan, Q. Kuang, J.Z. Zhou, X.J. Kong, Z.X. Xie, L.S. Zheng, J. Am. Chem. Soc. 135 (2013) 1926–1933.
[30] X. Zong, C. Sun, H. Yu, Z.G. Chen, Z. Xing, D. Ye, G.Q. Lu, X. Li, L. Wang, J. Phys. Chem. C 117 (2013) 4937–4942.
[31] S. Anandan, N. Ohashi, M. Miyauchi, Appl. Catal. B: Environ. 100 (2010) 502–509.
[32] G.A.S. Josephine, A. Sivasamy, Appl. Catal. B: Environ. 150–151 (2014) 288–297.
[33] J.-C. Sin, S.-M. Lam, I. Satoshi, K.-T. Lee, A.R. Mohamed, Appl. Catal. B: Environ. 148–149 (2014) 258–268.
[34] S.A. Ansari, M.M. Khan, S. Kalathil, A. Nisar, J. Lee, M.H. Cho, Nanoscale 5 (2013) 9238–9246.
[35] J. Wang, Z. Wang, B. Huang, Y. Ma, Y. Liu, X. Qin, X. Zhang, Y. Dai, ACS Appl. Mater. Interfaces 4 (2012) 4024–4030.

[36] J. Xu, X. Yang, H. Wang, X. Chen, C. Luan, Z. Xu, Z. Lu, V.A. Roy, W. Zhang, C.S. Lee, Nano Lett. 11 (2011) 4138–4143.
[37] L.-C. Chen, Y.-J. Tu, Y.-S. Wang, R.-S. Kan, C.-M. Huang, J. Photochem. Photobiol. A: Chem. 199 (2008) 170–178.
[38] L. Luo, W. Tao, X. Hu, T. Xiao, B. Heng, W. Huang, H. Wang, H. Han, Q. Jiang, J. Wang, Y. Tang, J. Power Sour. 196 (2011) 10518–10525.
[39] A.B. Patil, K.R. Patil, S.K. Pardeshi, J. Solid State Chem. 184 (2011) 3273–3279.
[40] C. Wang, Y. Wang, G. Zhang, C. Peng, G. Yang, Phys. Chem. Chem. Phys. 16 (2014) 3771–3776.
[41] A.P. Bhirud, S.D. Sathaye, R.P. Waichal, L.K. Nikam, B.B. Kale, Green Chem. 14 (2012) 2790–2798.
[42] S. Sun, X. Chang, X. Li, Z. Li, Ceram. Int. 39 (2013) 5197–5203.
[43] C. Wu, Appl. Surf. Sci. 319 (2014) 237–243.
[44] E.S. Tuzemen, K. Kara, S. Elagoz, D.K. Takci, I. Altuntas, R. Esen, Appl. Surf. Sci. 318 (2014) 157–163.
[45] D.Z. Zhou, B. Li, H.L. Wang, M. Salik, H.H. Wu, Z.F. Hu, S. Gao, Y.F. Peng, L.X. Yi, X.Q. Zhang, Y.S. Wang, Appl. Surf. Sci. 305 (2014) 474–476.
[46] D. Zhang, J. Gong, J. Ma, G. Han, Z. Tong, Dalton Trans. 42 (2013) 16556–16561.
[47] S. Cho, J.-W. Jang, J.S. Lee, K.-H. Lee, CrystEngComm 12 (2010) 3929–3935.
[48] O. Haibo, H.J. Feng, L. Cuiyan, C. Liyun, F. Jie, Mater. Lett. 111 (2013) 217–220.
[49] Y.G. Lin, Y.K. Hsu, Y.C. Chen, L.C. Chen, S.Y. Chen, K.H. Chen, Nanoscale 4 (2012) 6515–6519.
[50] S. Liu, C. Li, J. Yu, Q. Xiang, CrystEngComm 13 (2011) 2533–2541.
[51] F. Wang, L. Liang, L. Shi, M. Liu, J. Sun, Dalton Trans. 43 (2014) 16441–16449.
[52] A.B. Patil, K.R. Patil, S.K. Pardeshi, J. Hazard. Mater. 183 (2010) 315–323.
[53] Y. Sun, T. He, H. Guo, T. Zhang, W. Wang, Z. Dai, Appl. Surf. Sci. 257 (2010) 1125–1128.
[54] H. Zhang, Z. Tao, W. Xu, S. Lu, F. Yuan, Comput. Mater. Sci. 58 (2012) 119–124.
[55] J. Zhang, P. Zhou, J. Liu, J. Yu, Phys. Chem. Chem. Phys. 16 (2014) 20382–20386.
[56] M.D. Segall, P.J.D. Lindan, M.J. Probert, C.J. Pickard, P.J. Hasnip, S.J. Clark, M.C. Payne, J. Phys.: Condens. Matter. 14 (2002) 2714.
[57] J.P. Perdew, K. Burke, M. Ernzerhof, Phys. Rev. Lett. 77 (1996) 3865.
[58] J.P. Perdew, Y. Wang, Phys. Rev. B: Condens. Matter Mater. Phys. 45 (1992) 13244.
[59] J. Yu, P. Zhou, Q. Li, Phys. Chem. Chem. Phys. 15 (2013) 12040–12047.
[60] P. Zhou, J. Yu, Y. Wang, Appl. Catal. B: Environ. 142–143 (2013) 45–53.
[61] M. Horn, C.F. Schwerdtfeger, E.P. Meagher, Z. Kristallogr 136 (1972) 273.
[62] P. Zhou, J. Wu, W. Yu, G. Zhao, G. Fang, S. Cao, Appl. Surf. Sci. 319 (2014) 167–172.
[63] N.P. Herring, L.S. Panchakarla, M.S. El-Shall, Langmuir 30 (2014) 2230–2240.
[64] C.L. Hsu, Y.D. Gao, Y.S. Chen, T.J. Hsueh, ACS Appl. Mater. Interfaces 6 (2014) 4277–4285.
[65] L. Duan, P. Wang, X. Yu, X. Han, Y. Chen, P. Zhao, D. Li, R. Yao, Phys. Chem. Chem. Phys. 16 (2014) 4092–4097.
[66] J.P. Perdew, L. Mel, Phys. Rev. Lett. 51 (1983) 1884.
[67] X. Ma, Y. Dai, M. Guo, Y. Zhu, B. Huang, Phys. Chem. Chem. Phys. 15 (2013) 8722–8731.
[68] H. Zhang, L. Liu, Z. Zhou, Phys. Chem. Chem. Phys. 14 (2012) 1286–1292.